



CrossMark
click for updates

Cite this: *RSC Adv.*, 2015, 5, 56922

Branched peptide with three histidines for the promotion of Cu^{II} binding in a wide pH range – complementary potentiometric, spectroscopic and electrochemical studies†

Łukasz Szyrwił,^{*ab} József S. Pap,^{*c} Łukasz Szczukowski,^b Zsolt Kerner,^c Justyna Brasuń,^d Bartosz Setner,^e Zbigniew Szewczuk^e and Wiesław Malinka^b

Modifications in linear and cyclic peptides have been widely explored in relation with the associated effects on the coordination of Cu^{II}. Branching of peptides is yet another innovative conception to promote metal binding. The three dimensional (3D), quasi-tripodal structure of the new ligand, H-His-Dap(H-His)-His-NH₂ (3H, where Dap = L-2,3-diaminopropionic acid), which is created by the vicinal two N-terminal and one C-terminal functions of Dap allows triple-arm extension and offers new options in metal binding. A strategy is presented for the characterization of 3H focusing on the role of structural domains in Cu^{II} binding by comparison of analogous tetrapeptides that involve a varying number of His and Gly residues. Potentiometric, spectroscopic (UV-Vis, CD and EPR), mass spectrometric and electrochemical data indicate that in monomeric Cu^{II}-3H complexes the metal is bound with higher affinity compared to its structural domains indicating that the effect of 3D branching should be taken as an important factor for future studies on Cu^{II} peptide constructs.

Received 8th May 2015
Accepted 17th June 2015

DOI: 10.1039/c5ra08602g

www.rsc.org/advances

Introduction

Applications of designed peptides as specific ligands for copper have become expansive, including catalysts/electrocatalysts,¹ peptide based fluorescent metallo-probes,² chelating agents in neurodegenerative diseases³ and metal ion selective cell organelle targeting probes.⁴ This advancement in applications was largely promoted by the decades-long studies on copper-peptide complexes triggered by their relevance to biological systems.⁵ The number and position of certain residues in linear peptides, especially of histidine, substantially influences stability, coordination sphere and nuclearity of the complexes.^{5,6}

Branching of peptides potentially improves the proteolytic and serum stability,^{7,8} selective cell uptake properties,⁹ and also,

the metal binding efficiency.^{3,10} The improved targeting properties of this peptide family, compared to linear ones, was applied in gene transport processes, *e.g.*, His-rich peptides.¹¹ The unique, three dimensional (3D) structure was also improved to be more effective in multiple antigen peptides (MAP),¹² in anti-bacterial¹³ and in some therapeutic¹⁴ agents. Expanding the field of new, triple-arm peptides and their metal complex engineering can be crucial for the further development of those applications as well as, new enzyme mimicking centers,¹⁵ some drugs,¹⁶ radiopharmaceutics¹⁷ or novel artificial proteins.^{18,19}

Peptide branching with lysine promotes formation of dimeric complexes.³ In a recent study we demonstrated that dimerization at physiological pH can be suppressed with Dap-based branched peptides (Dap = L-2,3-diaminopropionic acid), H-Gly-Dap(H-Gly)-His-NH₂ (2GH) H-His-Dap(H-His)-Gly-NH₂ (2HG) (Fig. 1 2HG, 2GH).¹⁰ Here we report a new branched tetrapeptide that is also built on Dap and contains one C-terminal and two N-terminal histidine residues (Fig. 1, 3H).

From our previous study we learnt that placement of one histidine residue at the C-, or two at the N-terminal of Dap influences the Cu^{II} binding mode very differently. Here we discuss how the simultaneous presence of both domains will affect Cu^{II} complex stabilization, paying special attention to redox properties which may be of crucial importance, since inside the living cells Cu^I can be often stabilized. During the design of Cu-based biomimetics and bioinspired pharmaceuticals and in-cell metal transporters it is therefore

^aCNRS/UPPA, LCABIE, UMR5254, Helioparc, 2, av. Pr. Angot, F-64053 Pau, France. E-mail: lukasz.szyrwił@univ-pau.fr; Fax: +33-5594-07681; Tel: +33-5594-07739

^bDepartment of Chemistry of Drugs, Wrocław Medical University, ul. Borowska 211, 50-552 Wrocław, Poland

^cMTA Centre for Energy Research, Surface Chemistry and Catalysis Department, PO Box 49, H-1525 Budapest, Hungary

^dDepartment of Inorganic Chemistry, Wrocław Medical University, Borowska 211a, 50-552 Wrocław, Poland

^eFaculty of Chemistry, University of Wrocław, ul. F. Joliot-Curie 14, 50-383 Wrocław, Poland

† Electronic supplementary information (ESI) available: Fig. S1–S4 and Table S1. See DOI: 10.1039/c5ra08602g

desirable to consider the redox behavior of these systems. In addition, copper may occur in three oxidation states when ligated and usually one of the two possible single electron redox transitions, +3/+2 or +2/+1 between these states can be observed in copper enzymes and complexes with artificial ligands. This leads to rich redox chemistry²³ and catalysis, especially using molecular oxygen,²¹ and, in connection, the control of oxidative stress in living species.²²

Electrochemical studies on copper complexes rarely go beyond cyclic voltammetry (CV) performed either in an aprotic solvent or in water at a fixed pH.^{24–27} CV offers a wealth of experimental information and includes both kinetic and thermodynamic details of many chemical systems; on the other hand, pK_a values that substantially control short range proton transfer coupled to the electron transfer, and well defined formal potentials are only accessible when E vs. pH (Pourbaix) diagrams are considered.^{20,23} For this reason, after the initial CV experiments we also applied square-wave voltammetry (SWV) to address the pH-dependence of the $Cu^{II/III}$ transition and fitted the data with a modified Nernst equation in part relying on the speciation and spectroscopic information.

Potentiometric, spectroscopic and mass spectrometry data indicate effect of N- and C-terminal cooperation in stabilization of Cu binding. Results from electrochemistry also underline the advantages of the simultaneous presence of histidine residues on each arm of three branched peptides.

Experimental

Ligand synthesis

Materials. All Fmoc amino acids, including Fmoc-L-Dap(Fmoc)-OH used as a branching amino acid, solvents and

reagents were purchased from Iris Biotech GmbH (Marktredwitz, Germany) and used without further purification.

Peptide synthesis

The synthesis of the peptide H-His-Dap(H-His)-His-NH₂ was performed manually on the Rink Amide MBHA resin (loading: 0.52 mM g⁻¹) in a polypropylene syringe reactor (Intavis AG, Köln, Germany) equipped with polyethylene filter, according to the standard Fmoc (9-fluorenylmethoxycarbonyl) solid phase synthesis procedure. TBTU (*O*-(benzotriazol-1-yl)-*N,N,N',N'*-tetramethyluronium tetrafluoroborate) was used as a coupling reagent (3 equivalents). Oxyma Pure (ethyl-2-cyano-2-(hydroxyimino)acetate) (3 equivalents) and DIPEA (*N,N*-diisopropylethylamine) (6 equivalents) were used as additives. DMF (*N,N*-dimethylformamide) was used as solvent. Each coupling step was performed for 2 h. After removal of the Fmoc-protecting groups, from the diaminopropionic acid derivative, attached to the resin, with 25% piperidine in DMF, a mixture of Fmoc-His(Trt)-OH/TBTU/Oxyma Pure/DIPEA (6 equivalents of each reagent) in DMF was added and stirred for 24 h. The end of a coupling was confirmed by the Kaiser test. The peptide was cleaved from the resin simultaneously with the side chain deprotection using a solution of TFA/H₂O/TIS (95/2.5/2.5, v/v/v) at room temperature for 2 h and purified by semi-preparative RP-HPLC.

Purification and mass spectrometry analysis

The peptide was purified by the RP-HPLC using a Varian ProStar (Palo Alto, CA, California) with UV detection (210 nm and 280 nm) on a TSKgel ODS-120T 12TG08eh004 column (215 × 30.0 mm, 10 μm) equipped with a TSKguard column ODS (21,5 × 7.5 mm, 10 μm), with a gradient elution of 0–80% *B* in *A* (*A* = 0.1% TFA in water; *B* = 0.1% TFA in acetonitrile/H₂O, 4 : 1) for 40 min (flow rate 7 mL min⁻¹). The main peak, corresponding to the peptide H-His-Dap(H-His)-His-NH₂, was collected and the fraction was lyophilized. All spectrometric experiments for synthesis product identification were performed on a Bruker micrOTOF-Q mass spectrometer (Bruker Daltonics, Bremen, Germany) equipped with an ESI source. Analyte solutions (1 μg in 1 mL of 50 : 50 acetonitrile–water mixture containing 0.1% HCOOH) were pumped at a rate of 2 μL min⁻¹. The instrument was operated in the positive ion mode and calibrated before each analysis with the Tunemix™ mixture (Agilent Technologies, Santa Clara, USA) in quadratic method. For the MS spectra analysis, the Bruker Compass Data Analysis 4.0 software was used. Sophisticated Numerical Annotation Procedure (SNAP) algorithm was used for finding peaks. The measured m/z for H-His-Dap(H-His)-His-NH₂ (3H) of [M + H]⁺ ion was 515.2632 (calculated 515.2632).

Potentiometric studies

Peptide protonation and Cu^{II} complex stability constants were calculated from three titration curves carried out over the pH range 2.5–11.0 at 298 K under argon atmosphere. Ligand concentration was set in a range of 1 × 10⁻³ to 1.5 × 10⁻³ M. Metal-to-ligand ratio was 0.82 : 1, 0.85 : 1 and 0.95 : 1. The pH-metric titrations were performed in 0.1 M KCl on a Metrohm

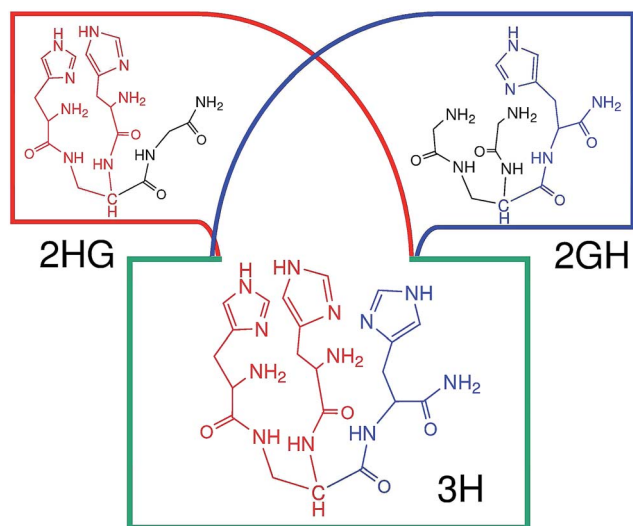


Fig. 1 Graphical presentation of combining two 2,3-diaminopropionic branched peptides in one that contains both metal binding histidine domains. The two N-terminal peptide arms are marked with red and the C-terminal arm is marked with blue. 2HG = H-His-Dap(H-His)-Gly-NH₂, 2GH = H-Gly-Dap(H-Gly)-His-NH₂ and 3H = H-His-Dap(H-His)-His-NH₂ peptides.

titrator using a Mettler Toledo InLab® Micro combined electrode calibrated for hydrogen ion concentration using HCl. The stability constants were calculated with HYPERQUAD 2013.²⁸ Standard deviations quoted were computed with the same software and refer to random errors only.

Spectroscopic studies (UV-Vis, CD, EPR)

Absorption spectra of Cu^{II} complexes were recorded on a PerkinElmer Lambda 25 spectrophotometer in 1 and 0.5 cm path length quartz cells. All UV-Vis spectra were collected in the 300–900 nm range. Circular dichroism (CD) spectra were recorded on a JASCO J 750 spectropolarimeter in the 250–900 nm range, using 1 and 0.1 cm cuvettes. Spectroscopic measurements were carried out at 298 K, at concentrations from 0.8 to 1.4 × 10⁻³ M and M : L = 1 : 1. Electron paramagnetic resonance (EPR) spectra were measured on a Bruker Elexsys 500 spectrometer operating at the X-band frequency (~9.7 GHz) at 123 K using narrow quartz capillaries to reduce the dielectric loss of the cavity. The ligand concentration was adjusted to 1 to 1.5 × 10⁻³ M in 30% (v/v) polyethylene glycol/water solution. Data from X-band EPR spectroscopy have been extracted by simulation of the experimental spectra taken at different pH values, at 123 K. For further details of the simulation method see ref. 10.

Mass spectrometry measurements

High-resolution mass spectra were obtained on a Bruker micrQ-FTMS spectrometer. Electrospray ionization (ESI-MS) mass spectra were measured in the positive ion mode. Before each run the instrument was calibrated externally with the Tunemix™ mixture. The ion source parameters were as follows: dry gas – nitrogen, temperature 170 °C, transfer time 120 ps, collision voltage –1.0 eV. The sample was dissolved in aqueous solution while the pH was adjusted with ammonium acetate to pH 4.5 and 6.8. The peptide concentration was in the 10⁻⁵ to 10⁻⁴ M range. The solution was infused at a flow rate of 3 μL min⁻¹. Simulations of the isotopic patterns were calculated using Bruker Data Analysis 4.0 software.

Electrochemistry

Cyclic voltammetry (CV), chronoamperometry (CA) and square-wave voltammetry (SWV) measurements were performed on a SP-150 potentiostat (BioLogic) equipped with a low-current unit. A standard three-electrode setup was used including a glassy carbon working electrode (GC, 0.072 cm²), Pt auxiliary electrode (~2 cm²) and Ag/AgCl (3 M KCl) reference electrode. The cell was modified to accommodate a pH microelectrode (Mettler-Toledo). The working electrode was carefully rinsed, polished and rinsed again right before each measurement (note that unpolished GC electrodes provide biased results, especially with peptides, for further information see ref. 29 and 30). The cell was kept under argon throughout the measurements, the O₂ level was checked with an optical O₂ sensor (Ocean Optics NeoFox). SWV settings were: 0.73 mM Cu-3H, 100 mM NaClO₄ electrolyte, 25 °C, pulse width 10 ms (*f* = 50 Hz), step potential 0.2 mV, SW pulse height 25 mV. The raw current curves (net

current, $I_{\text{net}} = \text{forward minus reverse current, } I_{\text{for}} - I_{\text{rev}}$) were baseline corrected uniformly with fitted cubic baselines to obtain the curves plotted in Fig. 7. All salts were purchased from commercial sources and were of puriss p.a. grade.

Results and discussion

Potentiometric titration, ESI-MS and pH-dependence of UV-Vis, CD and EPR spectroscopy

Complex formation between 3H and Cu^{II} in a ~1 : 1 solution starts already at acidic pH and increasing the pH to 3.5 results in a dominant CuH₃L complex (Fig. 2 and Table 1). The observed UV-Vis parameters for this species are close to those where Cu^{II} is bound with {2N_{im}} donors.³¹ This finding is in good agreement with analysis of potentiometric data, since the $\log K_{\text{CuL}}^* = \log \beta_{\text{CuH}_3\text{L}} - \log \beta_{\text{H}_3\text{L}} = 6.21(1)$ is close to $\log K_{\text{CuL}}^*$ of complexes with {2N_{im}} proposed in the literature ($\log \beta^* = 6.4$ (ref. 32) or 6.48 (ref. 31)).

X-band EPR spectroscopic results (Table 2 and Fig. 3) support this speciation, indicating the presence of two additional species to Cu_{aq}^{II} up to pH ~4.5 (Fig. 2). It is apparent from the experimental X-band EPR spectra that these *S* = 1/2 species give axial signal with $g_{\parallel} > g_{\perp} > 2.0$, but lower than *g*-values for Cu_{aq}^{II}. The characteristic $A_{\parallel}^{\text{Cu}} \gg A_{\perp}^{\text{Cu}}$ splitting pattern is typical for d_{x²-y²} ground state.³³ More precise *g*-tensors, hyperfine (hf) and superhyperfine (shf) coupling parameters were extracted by simulation of the spectra. The simulated component spectra for the contributing species at a given pH were fitted by optimization of the typical couplings of the unpaired electron to the ⁶³Cu and ⁶⁵Cu nuclei (*I* = 3/2). Shf coupling to nitrogen nuclei (¹⁴N, *I* = 1) can be expected for the copper-peptide complexes. Although the shf couplings to different numbers of equal nitrogen nuclei (Table 2) in the equatorial positions at lower pH remain unresolved, they still contribute to the improvement of the fittings. Rhombic anisotropy, *e.g.*, splitting of g_{\parallel} to g_x and g_y , at a varying level occurs in the investigated pH range (from 3 to 10) indicating distortion of the elongated octahedral (or square-

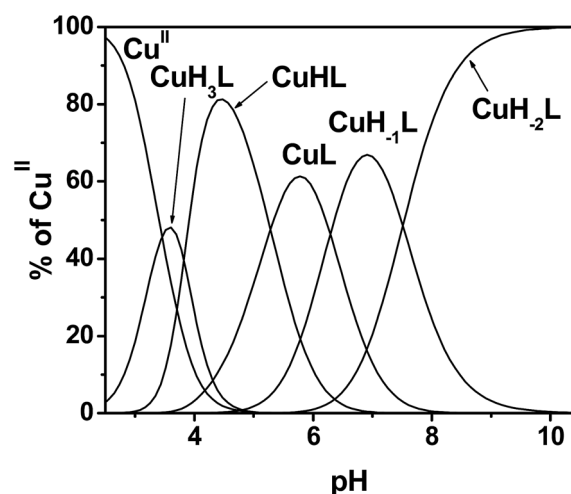


Fig. 2 Speciation diagram for the system containing Cu^{II} and 3H, [Cu^{II}] = 1 × 10⁻³ M, 1Cu^{II} : 1L (where L = 3H).

Table 1 The logarithms of the protonation constants ($\log \beta_{\text{HxL}}$) and stability constants ($\log \beta_{\text{CuHL}}$) for Cu^{II} complexes with 3H, UV-Vis and CD spectroscopic parameters for the respective species ($T = 298 \text{ K}$, $I = 0.1 \text{ M KCl}$)

Species	Potentiometry		UV-Vis	CD
	$\log \beta$	$\log K$	(λ [nm], ϵ [$\text{M}^{-1} \text{ cm}^{-1}$])	(λ [nm], $\Delta\epsilon$ [$\text{M}^{-1} \text{ cm}^{-1}$])
H_5L	30.69(3)	4.47(2)		
H_4L	26.22(3)	5.28(2)		
H_3L	20.94(3)	6.17(2)		
H_2L	14.77(2)	6.99(2)		
HL	7.78(3)			
CuH_3L	27.16(1)		670, 29	
CuHL	19.51(1)	5.28(2)	538, 60	562, -0.37 487, 0.15 311, 0.45 272, sh
CuL	14.23(3)	6.29(2)	532, 91	562, -0.60 478, 0.21 311, 0.97 272, sh
CuH_{-1}L	7.95(3)	7.51(3)	530, 98	563, -0.61 478, 0.22 308, 1.23 271, sh
CuH_{-2}L	0.43(4)		528, 103	561, -0.64 480, 0.23 309, 1.24 271, sh

based pyramid) geometry. In particular, the EPR parameters for CuH_3L corroborate other spectroscopic results. In the pH range 4.5–5.8 the CuHL and CuL species dominate (Fig. 2). The switch between the 2GH and 2HG domains (Fig. 1), more specifically the histidine at the C-terminal arm of 2GH starts to play critical role in Cu^{II} binding when pH is increased (Fig. 4 and S1†).

The ESI-MS results carried out at pH 6.8 confirmed the exclusive occurrence of monomeric complex in case of $\text{Cu} : \text{L}$ molar ratios of 0.4 : 1.0 and 0.7 : 1.0 (Fig. 5). The observed Cu–L signal pattern corresponds to two single charged ions with the molecular formula $\text{Cu}^{\text{II}}[\text{C}_{21}\text{H}_{29}\text{N}_{12}\text{O}_4]^+$ and $\text{Cu}^{\text{I}}[\text{C}_{21}\text{H}_{30}\text{N}_{12}\text{O}_4]^+$, which is in agreement with the formation of a 1 : 1 Cu–3H complex. Also, the linear increase in absorption near 529 nm supports occurrence of equimolar complexes in the range of Cu^{II} equivalent from 0–1 (Fig. S2†).

The UV-Vis absorption maximum (Cu d–d transition) shifts from 670 nm (associated with CuH_3L) to 538 and 532 nm associated with the CuHL and CuL, respectively (Table 1). This observation supports that in CuHL and CuL the metal ion is bound by 4N equatorial donor sets.³⁴ This is in agreement with the EPR spectroscopy parameters which indicate 4 nitrogen donors in the equatorial plane (Table 2 and Fig. 3). The $\log K$ correlated to the change of CuHL to CuL is 5.28(2). This observation as well as a shift in $\Delta\epsilon$ near 311 nm in the CD spectra suggest the involvement of an amide donor in the CuL complex, in addition, the EPR and UV-Vis data indicate that both species, CuHL and CuL have 4 nitrogen donor set with a very similar ligand field.

Based on the known Cu–peptide complex structures at pH 4.5–5.8 with linear^{5,6} and cyclic peptides³⁵ it could be proposed that in 3H at least eight nitrogen donors arranged in a three dimensional net are available for Cu^{II} binding, including 5 and 6 member chelate forming sites (Fig. S1a†). This allows for exchange of nitrogen donors as pH changes. In order to understand the potential role of structural motifs in metal binding the partial structural analogs to 3H were used in further comparisons (Fig. S1b–d†).

The 2HG peptide (Fig. S1b†), which contains Gly instead the C-terminal His residue of 3H, in the 4.5–5.5 pH range binds Cu^{II} by its N-terminal fork.¹⁰ The UV-Vis ($\lambda/\epsilon = 620/100$) and CD ($\lambda/\Delta\epsilon = 668/074$, $321/-0.41$) spectroscopic parameters for 2HG supported a 3N complex. The data for CuHL ($L = 3\text{H}$) in the same pH range are very different and consistent with a 4N environment (Tables 1 and 2). This difference excludes the option of closely related metal coordination by 2HG and 3H in this pH range (Fig. S1b†).

The H-HVH-OH peptide represents the backbone peptide chain of 3H (Fig. S1c†). The spectroscopic parameters for the corresponding Cu^{II} complexes with H-HVH-OH and 3H are also incompatible. In case of H-HVH-OH at pH 4.5–5.5 two complexes, CuHL and CuL ($L = \text{H-HVH-OH}$) were observed. The UV-Vis (λ/ϵ) parameters, 690/26 and 630/46, support 3N and 4N complexes, respectively³⁶ and are different from those observed for CuHL ($L = 3\text{H}$). The difference between the above listed data negates the hypothesis that the N- and C-terminal backbone arms of 3H (Fig. S1c†) are unaccompanied in the binding of Cu^{II} in this pH region.

Finally, for 2GH, in which both N-terminals are Gly residues, instead of the His residues for 3H (Fig. S1d†), the UV-Vis

Table 2 EPR parameters for the pH-dependent Cu–3H species and Cu^{IIa}

	Cu^{2+}	CuH_3L	"CuHL + CuL" ^b	CuH_{-1}L	CuH_{-2}L
g_{\parallel} (g_z)	2.417	2.3010	2.1948	2.1865	2.1906
g_{\perp} (g_x, g_y)	2.0826	2.0569, 2.0726	2.0407, 2.0544	2.0387, 2.0536	2.0407, 2.0511
$A_{\parallel}^{\text{Cu}}$ (A_z^{Cu})	129	168	193	198	196
A_{\perp}^{Cu} ($A_x^{\text{Cu}}, A_y^{\text{Cu}}$)	4	7, 8	9, 17	11, 21	14, 27
$a_{\parallel}^{\text{Nc}}$	—	8 (2N)	8 (4N)	8 (4N)	8 (4N)
a_{\perp}^{N} ($a_x^{\text{N}}, a_y^{\text{N}}$)	—	11, 9 (2N)	11, 12 (4N)	14, 15 (4N)	11, 14 (4N)

^a $[A] = 10^{-4} \text{ cm}^{-1}$. ^b CuHL and CuL were considered with the same parameters. ^c Estimation from unresolved structures (the effect is comparable to line broadening).

parameters, (λ/ϵ) 529/98, in the respective pH range were assigned to CuH_{-1}L . In this complex the $\{\text{NH}_2, 2\text{N}^-, \text{N}_{\text{im}}\}$ donor set is expected.¹⁰ The differences in (λ/ϵ) 538/65 from CuHL ($L = 3\text{H}$) don't support hypothesis about exactly the same coordination mode, however, strong similarity is observed in the CD spectra corresponding to CuL indicating the special role of the

C-terminal arm (for 2GH the respective data are $(\lambda/\Delta\epsilon)$ 568/−0.58, 481/0.23, 305/1.28 and 270/−2.05). This close resemblance indicates structural similarities between Cu-2GH and Cu-3H in this pH region.³⁷

Based on the presented information we conclude that even the presence of two N-terminal His arms in 3H peptide is insufficient to force out the C-terminal His from the coordination sphere of Cu^{II} . It follows that the C-terminal localization of His is strongly desirable for Cu^{II} binding already at slightly acidic pH.

As a summary, it can be proposed that all three arms should participate in Cu^{II} coordination either by direct metal ligation or by the support of a hydrogen bond network causing very little spectroscopic differences between the CuHL and CuL .^{38,39}

Formation of CuH_{-1}L (Fig. 2 pH 6–7) is accompanied by moderate changes in UV-Vis, CD and also EPR spectroscopy (Tables 1 and 2). The spectroscopic parameters are closely related to the Cu^{II} complex with 2GH which occurs in this pH range and in which the metal is bound by $\{\text{NH}_2, 2\text{N}^-, \text{N}_{\text{im}}\}$.¹⁰ This close similarity in the spectroscopic parameters indicates that 3H at pH 7 binds the Cu^{II} with the involvement of the C- and N-terminal main chain arms.

Interestingly, CuHL , CuL and CuH_{-1}L dominate in the pH range 4.5–7 where the switching between the affinity for Cu^{II} binding was calculated based on the stability constants (Fig. 4) and was also proved experimentally.¹⁰ Forming of these intermediate forms with spectroscopic parameters between those known for 2HG at low pH and 2GH at high pH is justified by switching of Cu^{II} binding between the corresponding branched peptide arms in 3H.

Further increase in pH up to 9 results in CuH_{-2}L ($L = 3\text{H}$). This process with $\log K = 7.51(3)$ does not induce significant spectroscopic changes and could be rationalized by the deprotonation of the non-coordinated amino group at one of the

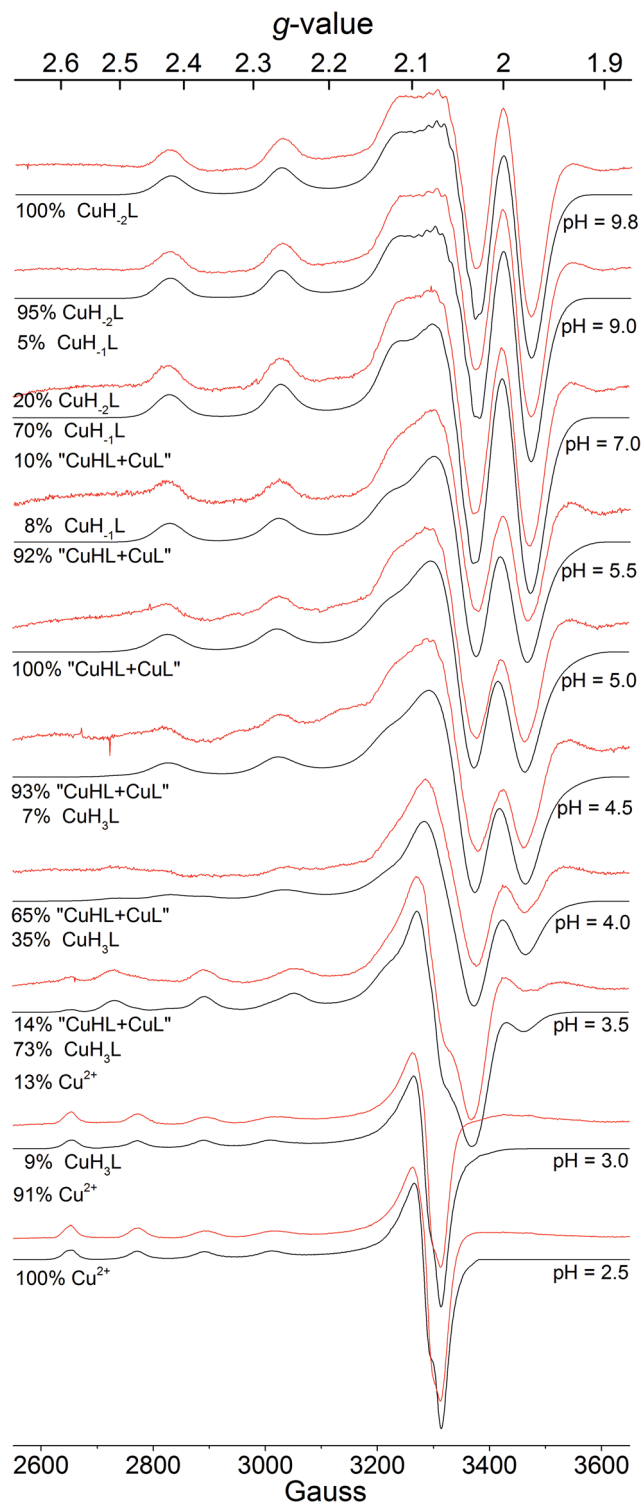


Fig. 3 Experimental (red) and simulated (black) EPR spectra at different pH for the $\text{Cu}^{\text{II}} : 3\text{H}$ system.

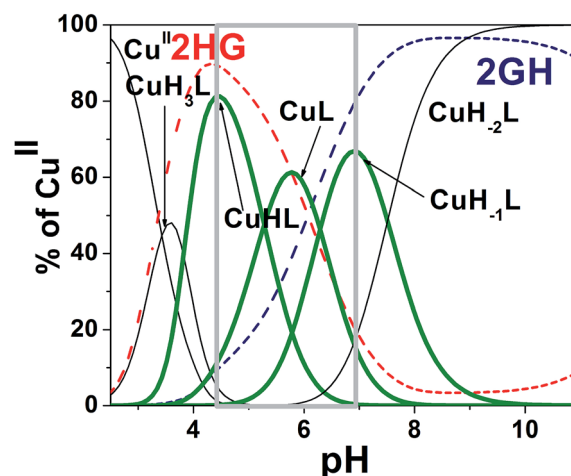


Fig. 4 Speciation diagram for Cu^{II} and 3H, dashed lines show curves of competition for Cu^{II} between the ligands 2HG (red) and 2GH (blue). The gray rectangle illustrates the region where the switching between branches that participate in Cu^{II} binding takes place as the respective complex species marked with green (CuHL , CuL and CuH_{-1}L) occur (the conditions of speciation and competition diagram: $[\text{Cu}^{\text{II}}] = [3\text{H}] = 1 \times 10^{-3} \text{ M}$, $[\text{Cu}^{\text{II}}] = [2\text{GH}] = [2\text{HG}] = 1 \times 10^{-3} \text{ M}$ respectively).

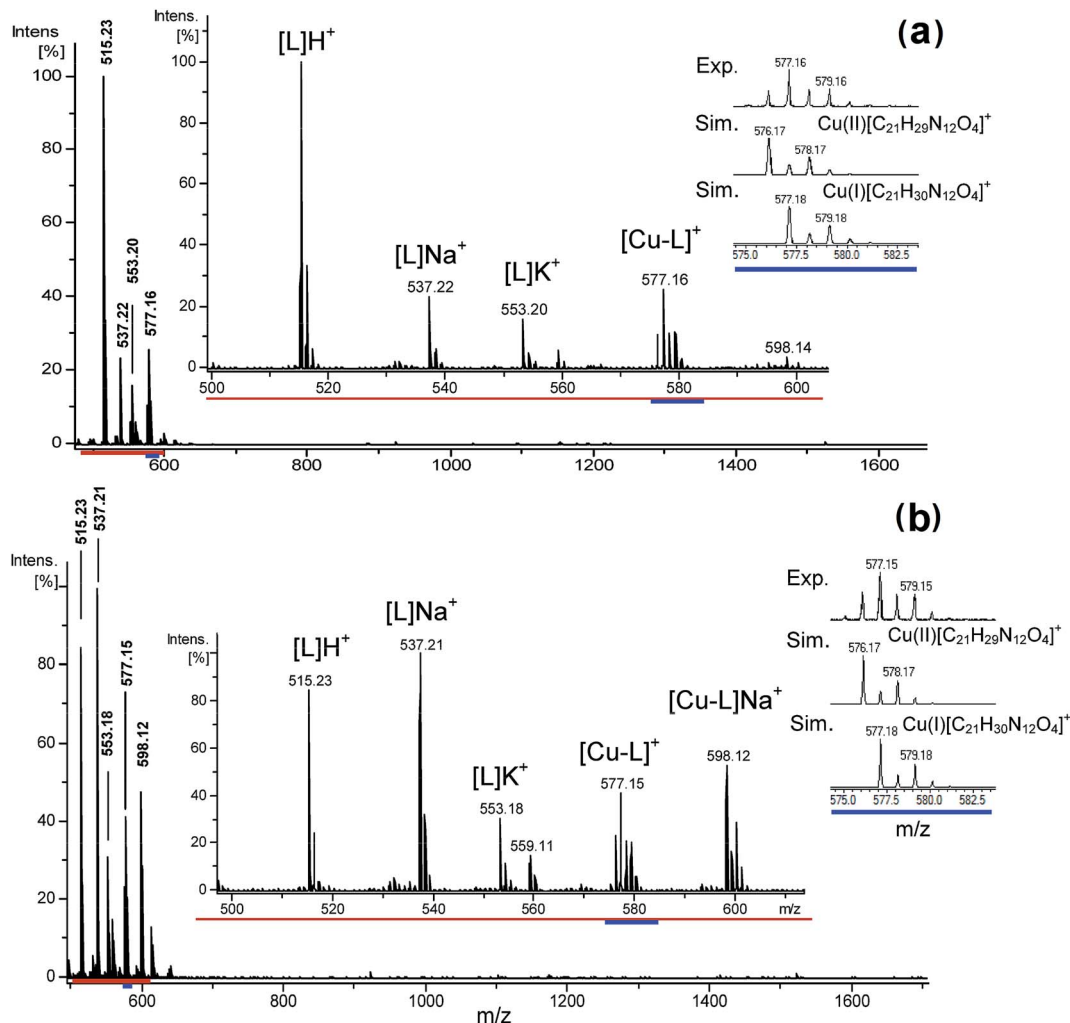


Fig. 5 The (+) ESI-MS spectrum of the Cu^{II}-L mixture at pH 6.8: (a) the Cu²⁺ : L ratio was 0.4 : 1.0 and (b) the Cu²⁺ : L ratio was 0.7 : 1.0 ($C_L = 0.8 \times 10^{-4}$ M, where L = 3H). Respective, blown up regions of spectra are marked with red and blue.

N-terminal branches, but nowise with any major changes in the first coordination sphere CuH₂L.

Competition study between Dap-based peptides

Fig. 6 shows the distribution of Cu^{II} among 2GH, 2HG and 3H, present in equal concentration. First of all, the Cu^{II} distribution switches between 2HG and 2GH (Fig. 6a and c) near pH 6. Up to pH 5 2HG, while above pH 7 the 2GH is the predominant ligand. Between pH 5 and 7 both peptides were found to be competitive (Fig. 6b).¹⁰ Somewhat surprisingly 3H is by far the best Cu^{II} complexing agent in the whole pH range, leaving behind both its N- (2HG) and C-terminal (2GH) domains (Fig. 1, S1b and d[†]). The coordination profile observed in case of 3H in the pH range up to 3.5 can be recognized as similar to 2HG (Fig. 1a), above pH 7 as similar to 2GH (Fig. 1b). In the region between 3.5 and 7 the involvement of all three branches in complexation of Cu^{II} is proposed. The observed extra stabilization may be rationalized by means of hydrogen bond network, similar to those observed for long, linear multi-histidine tags and histidine rich proteins.^{38,39}

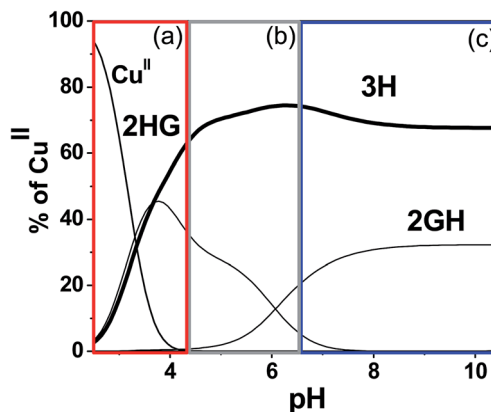


Fig. 6 Competition plot showing the distribution of Cu^{II} between 2GH, 2HG and 3H as a function of pH, [Cu^{II}] = [2GH] = [2HG] = [3H] = 1×10^{-3} M. Partitions denote those pH regions where spectroscopic parameters of 3H could be recognized as: (a) similar to 2HG (red), (b) 3H specific (2HG and 2GH competitive region), (c) similar to 2GH (blue).

Electrochemistry

The cyclic voltammograms (CVs) of the Cu–3H system were recorded at pH 7 and 8 (Fig. 7). This pH region is common condition for many of the enzymatic processes and biological environments. Under the given conditions 3H has high affinity for Cu^{II} (Fig. 6), but the question of redox stability remains open. Cathodic polarization of the GC working electrode yields a Faradaic current peak that shifts to more negative potential by ~40 mV with increasing pH to 8 (E'_{pc1}). On the reverse direction the anodic current peak occurs at considerably higher potential (E'_{pa1}) that is clear indication of a rapid background chemical process (electrochemical–chemical–electrochemical, ECE mechanism).

Such behavior is often observed for Cu^{III/I} transitions as the change in the redox state induces fundamental changes in the coordination number and geometry.⁴⁰ In the pH range of 6–8, Cu–3H complexes are present in three protonation states: Cu^{II}L, (and predominantly) Cu^{II}H₋₁L and Cu^{II}H₋₂L (Fig. 2). The pH-dependent spectroscopic features indicate (*vide supra*) that the coordination sphere – involving all three arms and consisting of 3 neutral N donor groups beside one N⁻ – transforms to {NH₂, 2N⁻, N_{im}} upon deprotonation of Cu^{II}L. Hureau *et al.* compared the redox features of [Cu^{II}(GHK)] (with 1N_{im}), [Cu^{II}(GHK)₂] (with 2N_{im}) and [Cu^{II}(GHK)(His)] (with 2N_{im}) (GHK = H-Gly-His-Lys-OH) at pH = 7.4 and suggested that addition of N_{im} will prevent losing the metal upon reduction,⁴¹ which otherwise leads to metallic copper deposition at the electrode. As a characteristic feature in CV they observed in the anodic direction a Cu⁰ to Cu^I oxidation-solubilization current peak beside the Cu^I to Cu^{II} peak.

All this information led us to propose a mechanism (Scheme 1) for the observed Cu^{III/I} redox cycle of the Cu–3H system. According to this mechanism, the irreversible, pH-dependent

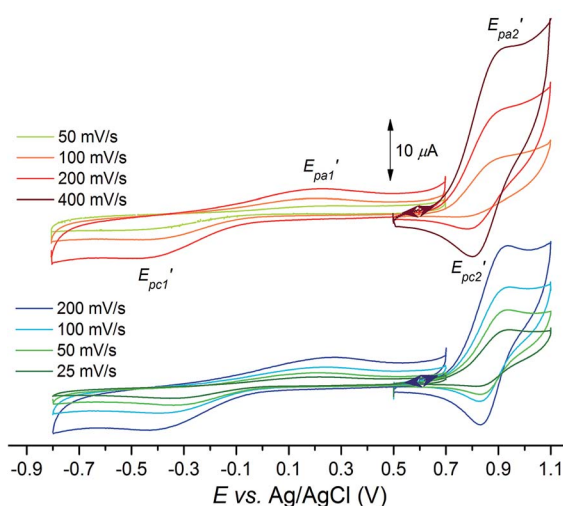
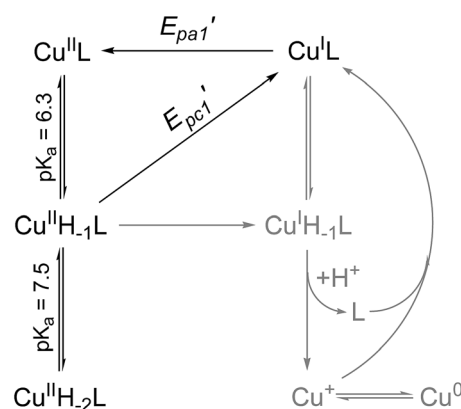


Fig. 7 Cyclic voltammograms of the Cu–3H system (2 mM in water, 0.1 M NaClO₄, under argon at 25 °C) at pH 7.0 (bottom) and at pH 8.0 (top) plotted on the same scale. The initial potential is 0.6 V for scans to both the anodic and cathodic directions (see blue and brown arrowheads).

E'_{pc1} can be assigned as the Cu^{II}H₋₁L to Cu^IL proton coupled electron transfer (PCET) reaction, while the E'_{pa1} to the Cu^IL to Cu^{II}L oxidation. The driving force of this mechanism is the possibility of intra-ligand translocation of copper upon reduction, allowed by the branched structure of 3H. Once in the Cu^IL form, the changed donor set will accommodate both Cu^I and Cu^{II}. One may suppose as an alternative assignment for E'_{pc1} that Cu^{II}H₋₁L is reduced directly to Cu^IH₋₁L. This species would most likely release Cu^I, or may again translocate Cu^I to the available His arms. The presence of free Cu^I would lead to oxidation-solubilization current peak, but this is not observed in the presented voltammograms. Therefore we suggest that, if free Cu^I is produced at all, it will be rapidly re-complexed by the neutral free ligand according to Scheme 1. The Cu–3H system exhibits a quasi-reversible Cu^{III/II} redox transition at pH 6.98 (Fig. 7, E'_{pa2} and E'_{pc2}) with $E_{1/2}$ of -0.88 V vs. Ag/AgCl, $\Delta E_p \sim 100$ mV and approximating $I_a = I_c$ at 200 mV s⁻¹. Chronoamperometry indicates that the current peaks associated with the Cu^{III/I} and Cu^{III/II} processes involve equal number of electrons (Fig. S3†). The $E_{1/2}$ value in comparison with literature examples where the equatorial binding plane of the complex is reported,^{1,40–42} suggests a {NH₂, 2N⁻, N_{im}} donor plane that is exactly what spectroscopic results indicate for Cu^{II}H₋₁L and Cu^{II}H₋₂L. However, when the pH is shifted to 8, even at 400 mV s⁻¹, I_a considerably exceeds I_c , showing that an EC_{rev} mechanism is operating accelerated by basic pH and competing with the electrochemical reduction of Cu^{III} on the CV timescale. A decrease in the peak potentials of ~30 mV could be estimated.

To our knowledge, information on the pH-dependence of Cu^{III/II} transitions in Cu-peptide complexes is rare in literature,^{23,43} despite that proton transfer processes coupled to redox transitions (PCET) are of key importance in biochemistry and catalysis.⁴⁴ Therefore we aimed to determine the Cu^{III/II} potential in the pH range from 7 to 8.8 for the Cu–3H system. In this range the Cu^{II}H₋₁L and Cu^{II}H₋₂L forms are predominant. Instead of CV we applied square-wave voltammetry (SWV) to determine the E^o values accurately, upon shifting the pH by small increments.¹ The E_{net} (potential of I_{net}) vs. pH plots will directly give Pourbaix diagrams, when reversibility terms of the



Scheme 1 Proposed processes that contribute to the observed Cu^{III/I} redox transitions in the CVs.

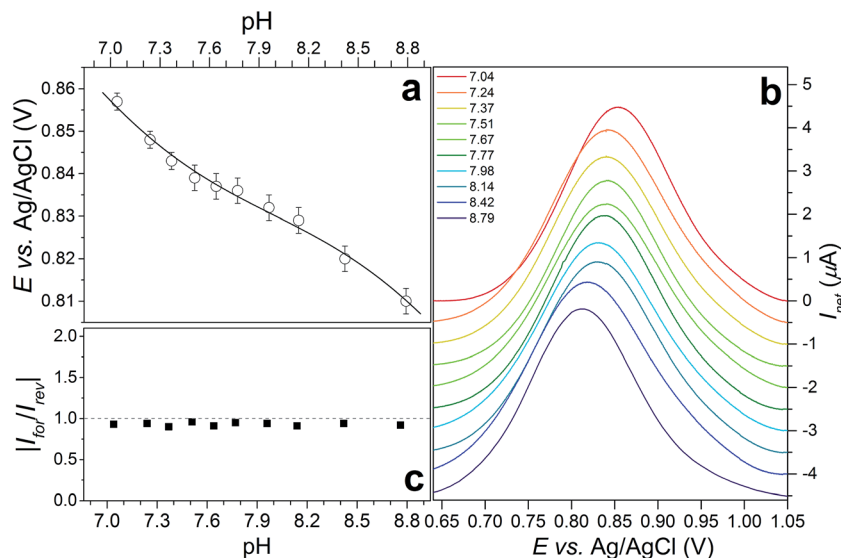
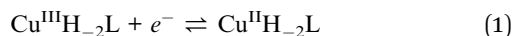


Fig. 8 (a) $\text{Cu}^{\text{III/II}}$ net potentials (E_{net}) determined by square-wave voltammetry (SWV) and plotted as a function of pH. The solid line represents a nonlinear regression curve fit to eqn (2) ($R^2 = 0.9857$, for parameters see Table 3). (b) Baseline corrected net current SW voltammograms of the Cu–3H system between pH 7.04 and 8.79. The potentials in Fig. 7a correspond to E_{net} of the baseline corrected net current traces, $I_{\text{net}} = I_{\text{for}} - I_{\text{rev}}$, where forward means the current response to the oxidation pulse while reverse to the reduction pulse. (c) Plot of the ratio of I_{for} and I_{rev} components as a function of pH. SWV conditions: 0.7 mM Cu–3H, 100 mM NaClO_4 , temperature 25.0 ± 0.1 °C, $t_p = 10$ ms ($f = 50$ Hz), step potential 0.2 mV, SW pulse amplitude 25 mV, 0.072 cm² GC working electrode, ~ 2 cm² Pt auxiliary electrode and Ag/AgCl (3 M KCl) reference electrode. All experiments were conducted under an Ar blanketing atmosphere, where O_2 concentration was <2 μM .

electrode process are fulfilled. Fig. 8 summarizes the SWV results for the $\text{Cu}^{\text{III/II}}$ transition (Table S1 sums the data, Fig. S4† illustrates reproducibility). In Fig. 8a the E_{net} data points are plotted against the pH generating a Pourbaix diagram for the $\text{Cu}^{\text{III/II}}$ process. Note that the $I_{\text{for}}/I_{\text{rev}}$ ratio approximating 1 (Fig. 8c) and symmetrical current peaks are landmarks of reversibility on the timescale of the experiment. Presuming that eqn (1) describes the electrochemical process, a modified Nernst eqn (2) can be written to explain the pH-dependence of E_{net} .⁴⁵ In this equation we presume the involvement of both the reduced (Cu^{II}) and oxidized (Cu^{III}) form in one protic equilibrium:

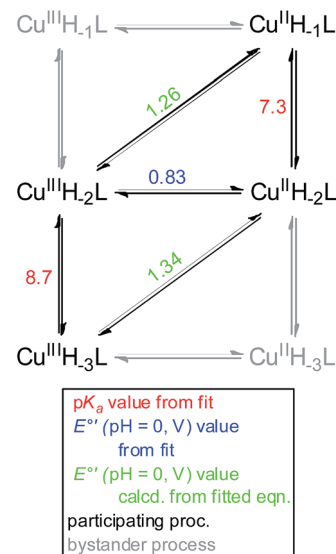


$$E_{\text{net}} = E^\circ(\text{Cu}^{\text{III}}\text{H}_{-2}\text{L}/\text{Cu}^{\text{II}}\text{H}_{-2}\text{L}, \text{pH} = 0) + 0.0591 \log \frac{K_a(\text{red}) + [\text{H}^+]}{K_a(\text{red})K_a(\text{ox}) + K_a(\text{red})[\text{H}^+]} - 0.0591\text{pH} \quad (2)$$

where $K_a(\text{red})$ is the acid dissociation constant of $\text{Cu}^{\text{II}}\text{H}_{-1}\text{L}$ to $\text{Cu}^{\text{II}}\text{H}_{-2}\text{L}$, $K_a(\text{ox})$ is the acid dissociation constant of $\text{Cu}^{\text{III}}\text{H}_{-2}\text{L}$ to

$\text{Cu}^{\text{III}}\text{H}_{-3}\text{L}$ and E° ($\text{Cu}^{\text{III}}\text{H}_{-2}\text{L}/\text{Cu}^{\text{II}}\text{H}_{-2}\text{L}$, pH = 0) is the formal potential of the process in eqn (1). Fit of eqn (2) to E_{net} data points yields the line in Fig. 8a and parameters as listed in Table 3.

The $\text{p}K_a(\text{red})$ is in satisfactory agreement with the $\log K = 7.51(3)$ value for the $\text{Cu}^{\text{II}}\text{H}_{-1}\text{L}$ form derived from potentiometry. The projections of the fitted function to pH = 0 (e.g., $E^\circ(\text{Cu}^{\text{III}}\text{H}_{-2}\text{L}/\text{Cu}^{\text{II}}\text{H}_{-2}\text{L}, \text{pH} = 0) + 0.0591\text{p}K_a(\text{red or ox})$) give $E^\circ(\text{Cu}^{\text{III}}\text{H}_{-2}\text{L}, \text{H}^+/\text{Cu}^{\text{II}}\text{H}_{-1}\text{L}, \text{pH} = 0)$ as 1.26 V and $E^\circ(\text{Cu}^{\text{III}}\text{H}_{-3}\text{L}, \text{H}^+/\text{Cu}^{\text{II}}\text{H}_{-2}\text{L}, \text{pH} = 0)$ as 1.34 V. These potentials along with the



Scheme 2 Processes operating in the pH range of the SWV study.

Table 3 Formal potential and $\text{p}K_a$ values derived from the fit of eqn (2) to experimental E_{net} vs. pH data for the $\text{Cu}^{\text{III/II}}$ redox transition

	Eqn (2)
$\text{p}K_a(\text{red})$	7.3(1)
$E^\circ(\text{Cu}^{\text{III}}\text{H}_{-2}\text{L}/\text{Cu}^{\text{II}}\text{H}_{-2}\text{L})$ vs. Ag/AgCl(v)	0.831(3)
$\text{p}K_a(\text{ox})$	8.7(1)

fit parameters can be assigned to equilibria, which are arranged into a stepladder scheme of the PCET processes (Scheme 2, protons and electrons are omitted for sake of simplicity).

The horizontal equilibria involve no change in protons (ET), while vertical ones no change in electrons (PT). The diagonal processes are assigned as multiple site electron-proton transfer (MS-EPT⁴⁴) processes, differing in their potential by $0.0591\text{p}K_{\text{a}}(\text{red or ox})$ from the value for the ET of 0.83 V. According to this scheme, the MS-EPT processes become favored for the Cu-3H system at pH below $\text{p}K_{\text{a}}(\text{red})$ and above $\text{p}K_{\text{a}}(\text{ox})$.

Conclusions

Our strategy to combine in one three dimensional branched peptide two structural motifs with maximal Cu^{II} binding efficiency in different ranges of pH, resulted in the design of the novel triple-arm peptide 3H. Our data demonstrate that this structure can significantly increase Cu^{II} binding affinity. The extra stabilization of Cu-3H complexes in comparison with analogues of the Cu^{II} binding domains indicate that all arms are involved in metal binding near the physiological pH, moreover, the C-terminal His residue is dominating.

Prolongation of the C-terminal peptide arm therefore can be recommended in order to functionalize the complex with, for example, anchoring moiety or peptide sequence targeting. Importantly, upon reduction of Cu^{II} to Cu^I bound to 3H no metal deposition was observed at the electrode, indicating that the ligand can retain Cu^I from dissociation. We attribute this behavior to the propensity of 3H to flexibly adopt its structure to altered redox conditions. This advantage of 3H is also traced in supporting a Cu^{III/II} redox transition among the very same conditions, separated by ~ 1.2 V from the Cu^{II} to Cu^I reduction. Our electrochemical investigations suggest that PCET processes play key role in redox-coupled structure switching. Surface anchoring of our complexes will be explored in upcoming studies.

This experience can be applied in the design of Cu^{II}-peptide based radiopharmaceuticals, metal sensors, peptide based Cu^{II} fluoroprobes and also applied in the catalytic/electrocatalytic multi histidine metallopeptides or artificial proteins. The presented Dap peptide frame and branching methodology may help achieve the desirable goal of elucidating the contribution of different aminoacids (donor groups) localized in different positions of three dimensional net to understand their role in copper binding and activity.

Acknowledgements

This study was supported by a Polish Foundation of Science within the POMOST program co-financed by the European Union within European Regional Development Fund (POMOST/2012-5/9). Support from the MTA through a János Bolyai Scholarship is also acknowledged (J. S. Pap).

Notes and references

- J. S. Pap, L. Szyrwił, D. Sranko, Z. Kerner, B. Setner, Z. Szewczuk and W. Malinka, *Chem. Commun.*, 2015, **51**, 6322–6324.
- T. R. Young, C. J. K. Wijekoon, B. Spyrou, P. S. Donnelly, A. G. Wedd and Z. Xiao, *Metallomics*, 2015, **7**, 567–578.
- A. Lakatos, B. Gyurcsik, N. V. Nagy, Z. Csendes, E. Wéber, L. Fülöp and T. Kiss, *Dalton Trans.*, 2012, **41**, 1713–1726.
- L. Szyrwił, M. Shimura, J. Shirataki, S. Matsuyama, A. Matsunaga, B. Setner, L. Szczukowski, Z. Szewczuk, K. Yamauchi, W. Malinka, L. Chavatte and R. Lobinski, *Metallomics*, 2015, DOI: 10.1039/c5mt00021a.
- H. Kozłowski, W. Bal, M. Dyba and T. Kowalik-Jankowska, *Coord. Chem. Rev.*, 1999, **184**, 319–346.
- I. Sóvágó, C. Kállay and K. Várnagy, *Coord. Chem. Rev.*, 2012, **256**, 2225–2233.
- C. Falciani, L. Lozzi, A. Pini, F. Corti, M. Fabbrini, A. Bernini, B. Lelli, N. Niccolai and L. Bracci, *Chem. Biol. Drug Des.*, 2007, **69**, 216–221.
- L. Bracci, C. Falciani, B. Lelli, L. Lozzi, Y. Runci, A. Pini, M. G. De Montis, A. Tagliamonte and P. Neri, *J. Biol. Chem.*, 2003, **278**, 46590–46595.
- G. A. Eggimann, S. Buschor, T. Darbre and J.-L. Reymond, *Org. Biomol. Chem.*, 2013, **11**, 6717–6733.
- L. Szyrwił, L. Szczukowski, J. S. Pap, B. Setner, Z. Szewczuk and W. Malinka, *Inorg. Chem.*, 2014, **53**, 7951–7959.
- Q. Leng and A. J. Mixson, *Nucleic Acids Res.*, 2005, **33**, e40.
- K. Sadler and J. P. Tam, *Rev. Mol. Biotechnol.*, 2002, **90**, 195–229.
- M. Stach, N. Maillard, R. U. Kadam, D. Kalbermatter, M. Meury, M. G. P. Page, D. Fotiadis, T. Darbre and J.-L. Reymond, *MedChemComm*, 2012, **3**, 86–89.
- S. P. Liu, L. Zhou, R. Lakshminarayanan and R. W. Beuerman, *Int. J. Pept. Res. Ther.*, 2010, **16**, 199–213.
- A. Esposito, E. Delort, D. Lagnoux, F. Djojo and J.-L. Reymond, *Angew. Chem., Int. Ed.*, 2003, **42**, 1381–1383.
- J. E. Wynn and W. L. Santos, *Org. Biomol. Chem.*, 2015, **13**, 5848–5858.
- J. L. Hickey, E. J. Simpson, J. Hou and L. G. Luyt, *Chem.–Eur. J.*, 2015, **21**, 568–578.
- T. Darbre and J.-L. Reymond, *Acc. Chem. Res.*, 2006, **39**, 925–934.
- A. G. Tebo and V. L. Pecoraro, *Curr. Opin. Chem. Biol.*, 2015, **25**, 65–70.
- D. B. Rorabacher, *Chem. Rev.*, 2004, **104**, 651–698.
- Copper-oxygen chemistry*, ed. K. D. Karlin and S. Itoh, Wiley, Hoboken-New Jersey, 2011, vol. 4.
- H. Kozłowski, A. Janicka-Klos, J. Brasun, E. Gaggelli, D. Valensin and G. Valensin, *Coord. Chem. Rev.*, 2009, **253**, 2665–2685.
- M. R. McDonald, F. C. Fredericks and D. W. Margerum, *Inorg. Chem.*, 1997, **36**, 3119–3124.
- P. Faller, C. Hureau, P. Dorlet, P. Hellwig, Y. Coppel, F. Collin and B. Alies, *Coord. Chem. Rev.*, 2012, **256**, 2381–2396.

- 25 K. P. Neupane, A. R. Aldous and J. A. Kritzer, *J. Inorg. Biochem.*, 2014, **139**, 65–76.
- 26 C. Hureau, H. Eury, R. Guillot, C. Bijani, S. Sayen, P.-L. Solari, E. Guillon, P. Faller and P. Dorlet, *Chem.–Eur. J.*, 2011, **17**, 10151–10160.
- 27 A. B. Grosas, P. Kalimuthu, A. C. Smith, P. A. Williams, T. J. Millar, P. V Bernhardt and C. E. Jones, *Neurochem. Int.*, 2014, **70**, 1–9.
- 28 P. Gans, A. Sabatini and A. Vacca, *Talanta*, 1996, **43**, 1739–1753.
- 29 B. W. Berry, M. C. Martínez-Rivera and C. Tommos, *Proc. Natl. Acad. Sci. U. S. A.*, 2012, **109**, 9739–9743.
- 30 *Electroanalytical Methods*, ed. F. Scholz, Springer-Verlag, Berlin, 2010.
- 31 C. Kállay, K. Várnagy, G. Malandrinos, N. Hadjiliadis, D. Sanna and I. Sòvágó, *Inorg. Chim. Acta*, 2009, **362**, 935–945.
- 32 A. Matera-Witkiewicz, J. Brasuń, J. Świątek-Kozłowska, A. Pratesi, M. Ginanneschi and L. Messori, *J. Inorg. Biochem.*, 2009, **103**, 678–688.
- 33 B. J. Hathaway, G. Wilkinson, R. D. Gillard and J. A. McCleverty, *Compr. Coord. Chem.*, 1987, **5**, 533–774.
- 34 E. Prenesti, P. G. Daniele, S. Berto and S. Toso, *Polyhedron*, 2006, **25**, 2815–2823.
- 35 J. Brasun, C. Gabbiani, M. Ginanneschi, L. Messori, M. Orfei and J. Swiatek-Kozłowska, *J. Inorg. Biochem.*, 2004, **98**, 2016–2021.
- 36 A. Myari, G. Malandrinos, Y. Deligiannakis, J. C. Plakatouras, N. Hadjiliadis, Z. Nagy and I. Sòvágó, *J. Inorg. Biochem.*, 2001, **85**, 253–261.
- 37 H. F. Stanyon, X. Cong, Y. Chen, N. Shahidullah, G. Rossetti, J. Dreyer, G. Papamokos, P. Carloni and J. H. Viles, *FEBS J.*, 2014, **281**, 3945–3954.
- 38 A. Jancsó, A. Kolozsi, B. Gyurcsik, N. V Nagy and T. Gajda, *J. Inorg. Biochem.*, 2009, **103**, 1634–1643.
- 39 J. Watly, E. Simonovsky, R. Wiczorek, N. Barbosa, Y. Miller and H. Kozłowski, *Inorg. Chem.*, 2014, **53**, 6675–6683.
- 40 C.-T. Lin, D. B. Rorabacher, G. R. Cayley and D. W. Margerum, *Inorg. Chem.*, 1975, **14**, 919–925.
- 41 B. Alies, B. Badei, P. Faller and C. Hureau, *Chem.–Eur. J.*, 2012, **18**, 1161–1167.
- 42 C. Hureau, L. Charlet, P. Dorlet, F. Gonnet, L. Spadini, E. Anxolabéhère-Mallart and J.-J. Girerd, *JBIC, J. Biol. Inorg. Chem.*, 2006, **11**, 735–744.
- 43 M.-T. Zhang, Z. Chen, P. Kang and T. J. Meyer, *J. Am. Chem. Soc.*, 2013, **135**, 2048–2051.
- 44 D. R. Weinberg, C. J. Gagliardi, J. F. Hull, C. F. Murphy, C. A. Kent, B. C. Westlake, A. Paul, D. H. Ess, D. G. McCafferty and T. J. Meyer, *Chem. Rev.*, 2012, **112**, 4016–4093.
- 45 P. Wardman, *J. Phys. Chem. Ref. Data*, 1989, **18**, 1637–1755.